Supporting Information for

Anti-stacking Dense Conversion of Solid Organic Sodium Salt Particles into Graphene with Excellent Electrode Performance

Huijuan Cui,[ab] Yanyan Zhu,[ab] Jianfeng Zheng, *[a] Suping Jia,[a] Zhijian Wang[a] and Zhenping Zhu * [a]

a, State Key Laboratory of Coal Conversion, Institute of Coal Chemistry, Chinese Academy of Sciences, Taiyuan, 030001, China.

b, University of Chinese Academy of Science, Beijing,100049, China.

E-mail: zhengjf@sxicc.ac.cn ; zpzhu@sxicc.ac.cn

This supplementary information containing

Materials and methods

Figures S1-S18

Table S1-S3

References 1-27

Materials and Methods

Synthesis of GFs. In a typical experiment, sodium acetate (1.5 g) was put in a small ceramic boat, which then was placed in a tubular quartz reactor. After the reactor was pre-heated up to desired temperature (700-1200 ^{o}C) in argon stream, the ceramic boat (originally laid at the up-stream cool zone of the reactor) was shifted to the constant temperature zone through moving the reactor to allow the starting materials decompose an ultrahigh heating rate. After a short-time reaction, typically one minute, the resulted black solids were moved out of the high-temperature zone by moving the reactor and allowed to gradually cool to room temperature. The black solids (as-prepared GFs) were collected for direct analyses or further purification treatment. The pure GFs were obtained by washing as-prepared GFs with deionized water fully to

remove the formed Na_2CO_3 and dried in a vacuum at 60 ^oC for 24 h. The synthesis conditions for other organic acid salts and pyrolysis temperature were similar. All the reagents were analytic grade and used as received, without further treatment.

Characterization of GFs. The morphologies of the as-synthesized graphene and GFs were investigated by field emission scanning electron microscopy (FESEM) (JSM-7001F, operated at 10 kV) and transmission electron microscopy (TEM) (JEM-2100F, operated at 200 kV). Atomic Force Microscope (AFM) was performed using a Nanoscope 4 instrument. Raman measurements were carried out on a LABRAM-HR Raman system with an excitation wavelength of 514.5 nm. The elemental composition of the products was studied by X-ray photoelectron spectroscopy (XPS) (AXIS ULTRA DLD, employing an Al Kα X-ray source). X-ray diffraction (XRD) were performed using Bruker D8 Advance X-Ray Powder Diffractometer with Cu Kα (λ=1.5406 Å) radiation. Fourier transformed infrared (FTIR) spectrum was obtained using a TENSOR27 infrared spectrometer. The measurement of the nitrogen adsorption isotherms was done with ASAP 2020 at 77.4 K to obtain the surface areas of GFs samples. The mass spectrometry (MS) was performed by a mass spectrometer (Pfeiffer Vacuum OmniStar), which was directly connected with synthesis reactor for in situ analyses of released gases during the reaction.

Electrochemical measurements:

Electrochemical measurements of QDSSCs.

Electrochemical impedance spectroscopy (EIS) was employed to investigate electrochemical behavior of the various counter electrodes for S^{2-}/S_x^{2-} redox system, using the symmetric cells which filled with the redox electrolyte (0.16 cm^2 in area) between two identical counter electrodes (see Figure S13a). The EIS measurements were performed at an electrochemical workstation (IM6ex, Zahner) under dark in a frequency range of 100 KHz ~ 100 mHz, with a zero potential applied across the dummy cell, a perturbation amplitude of 10 mV. The electrolyte was an methanol and water（v:v=7:3）solution of the mixture containing Na_2S (2 M), S (2 M) and KCl (0.2 M). The electrochemical parameters including series resistance (R_s), charge transfer resistance (R_{ct}) at electrode-electrolyte interface, and Nernst diffusion impedance (Z_N) are obtained by fitting the Nyquist plots with an equivalent circuit model (Figure S13b).

Fabrication of QDSSCs and the measurement of performances: TiO_2 films were prepared according to the method reported previously.[1]The GFs and RGO counter electrode were prepared referring to the method described elsewhere.[2] Briefly, the carbon materials (90 wt.%) and poly-vinylidenefluoride (10 wt.%) with desired amount were mixed and dissolved in N-methyl pyrrolidinone to form a uniform slurry by a full stirring. The counter electrodes were prepared by coating the slurry onto FTO glass by doctor blade method, followed by evaporating the solvent at 80℃ for 12 hours. Pt counter electrode was also fabricated with H_2PtCl_6 following the reported method.[3]

The QDSSCs were prepared referring to the previous method.[4] Chemical bath deposition was used to assemble the QDs on the TiO_2 films prepared above as described previously. CdS and CdSe QDs were in sequence deposited for 30 min and 5.5 h, respectively, at 10℃ in the dark. Finally, surface passivation with ZnS was conducted by alternately dipping into 0.1 M $Zn(CH_3COO)_2$ and 0.1 M Na_2S aqueous solution for 1 min for two cycles. The photoanode and counter electrode were assembled in a sandwich-type cell, penetrated with the methanol and H_2O (v:v=7:3) solution electrolytes, containing Na_2S (2 M), S (2 M) and KCl (0.2 M).

For photovoltaic testing, a solar light simulator (Oriel, 91192) was used to provide an illumination of 100 $mW \cdot cm^2$ (AM 1.5). A digital source meter (2400 Source Meter, Keithley Instruments Inc., USA) was used to record the current–voltage plots.

Electrochemical measurements of supercapacitor.

Working electrodes were fabricated by mixing GFs (95 wt.%) and polytetrafluoroethylene binder (5 wt.%). The mixture (2 mg) was pressed onto nickel foam current collectors to create electrodes. The prepared electrodes were vacuum dried at 60 °C for 10 h. Before electrochemical testing, the electrodes were soaked overnight in electrolyte. Electrochemical tests were performed in aqueous 6 M KOH electrolyte with a three-electrode system, in which platinum was the counter electrode and $Hg/HgCl_2$ was the reference electrode. The electrochemical performances were characterized by cyclic voltammetry (CV) galvanostatic charge/discharge and EIS

measurements. CV was conducted at an electrochemical workstation (CHI660D). Galvanostatic tests were performed using a galvanostatic charge/discharge device (LAND CT2001A). The EIS measurements were performed at an electrochemical workstation (IM6ex, Zahner) in a frequency range of 100 KHz ~ 100 mHz, with a perturbation amplitude of 10 mV.

Supplementary Figures

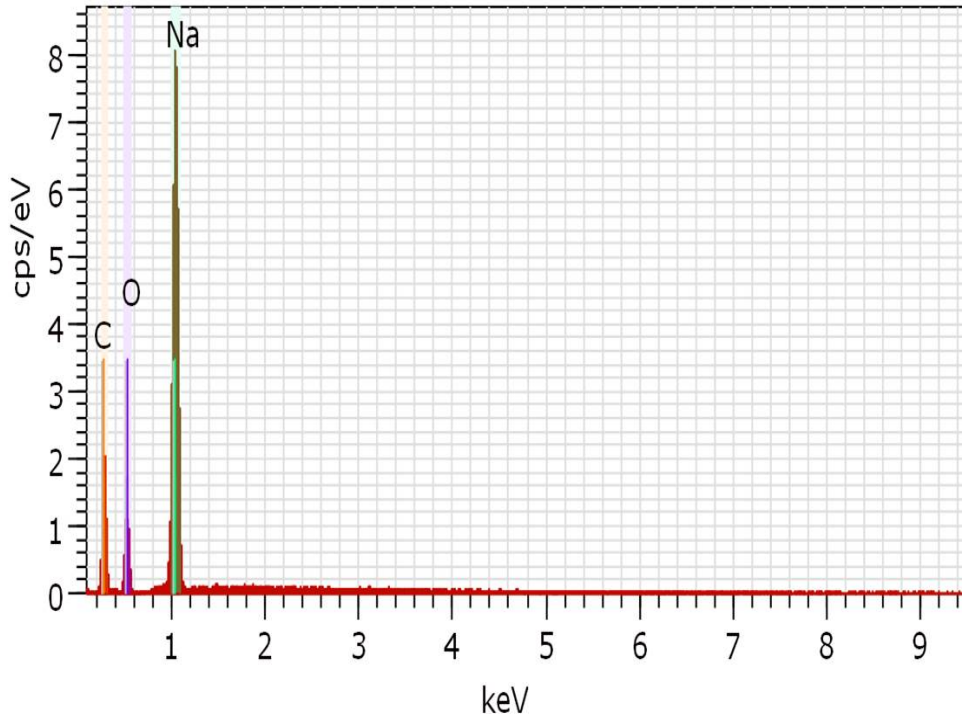

Figure S1. Energy dispersive X-ray spectrum of the as-prepared GFs from the fast decomposition of NaAc at 1200 ^{o}C.

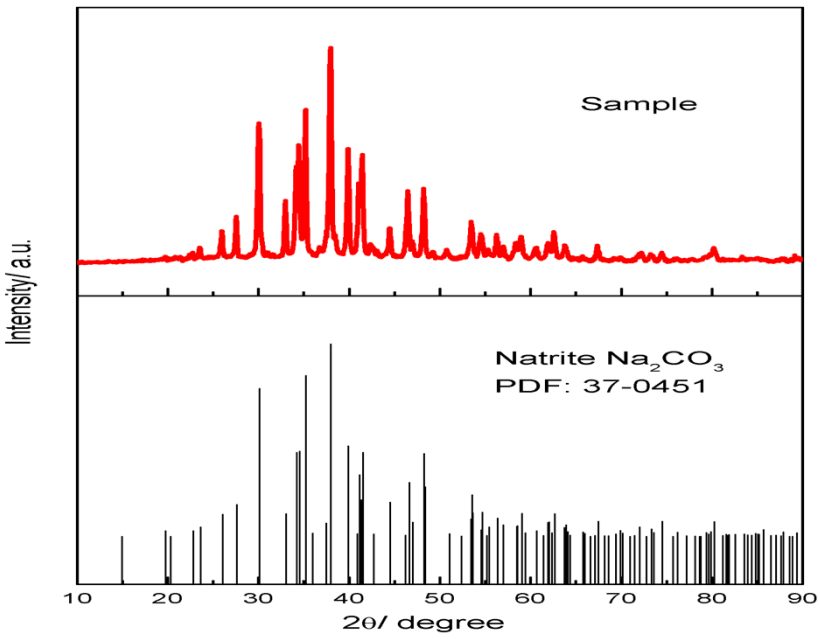

Figure S2. X-ray diffraction pattern of the as-prepared GFs from the fast decomposition of NaAc at 1200 °C. All the diffraction peaks of the as-prepared GFs can be readily indexed to natrite crystal phase of Na_2CO_3, indicating the generation of Na_2CO_3 during GFs formation.

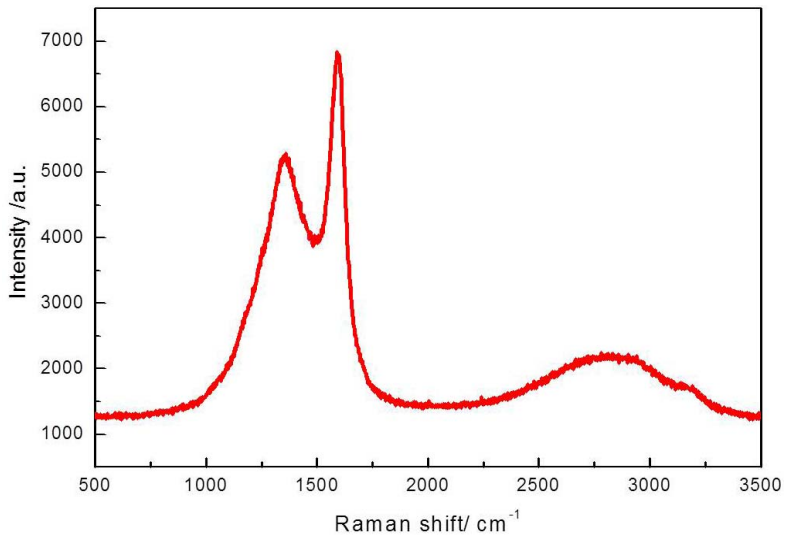

Figure S3. Raman spectrum of the GFs synthetized by the fast decomposition of

NaAc at 1200 °C. The bands at 1360 cm^{-1}, 1590 cm^{-1} and 2750 cm^{-1} are corresponding to the D, G and 2D bonds, respectively.[5] The I_{2D}/I_G is one of the methods to confirm the number of graphene layers.[6,7] The intensity ratio of the 2D to G peak being higher than 2, from 1 to 2, and lower than 1 indicate the monolayer, bilayer, and few layer graphene, respectively. The I_{2D}/I_G (0.35) of GFs is lower than 1 which indicates the GFs is a few layer graphene.

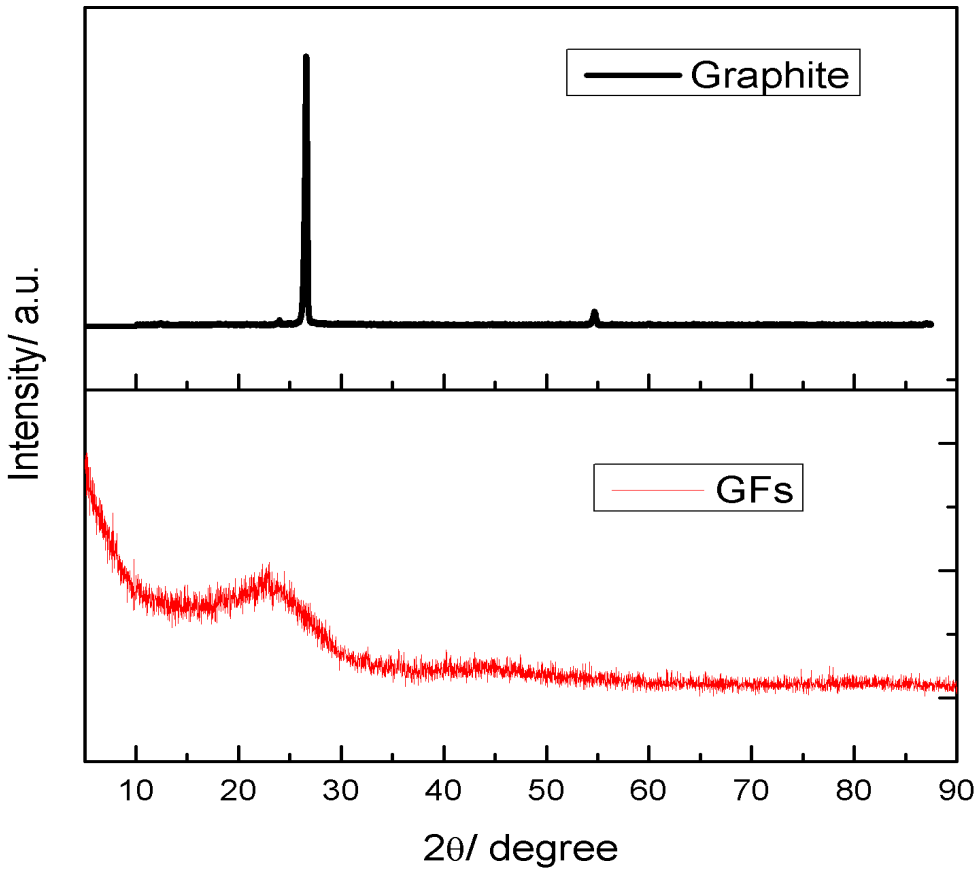

Figure S4. The XRD pattern of GFs and graphite. The GFs exhibited a pronounced peak at 24.2°, corresponding to the interlayer spacing of 0.367 nm, further indicative of developing graphitic structures. The result was consistent with other graphene materials.[8,9] Nevertheless, compared with the well-ordered graphite (Aladdin

Industrial Corporation, 26.3°, 0.344 nm), the peak was relatively weak and broadened. These phenomena revealed a decreased degree of graphitization and crystallinity[8,9] which may be due to the presence of oxygen. Together with these results of TEM, AFM and Raman spectrum, the obtained GFs was not graphite but graphene.

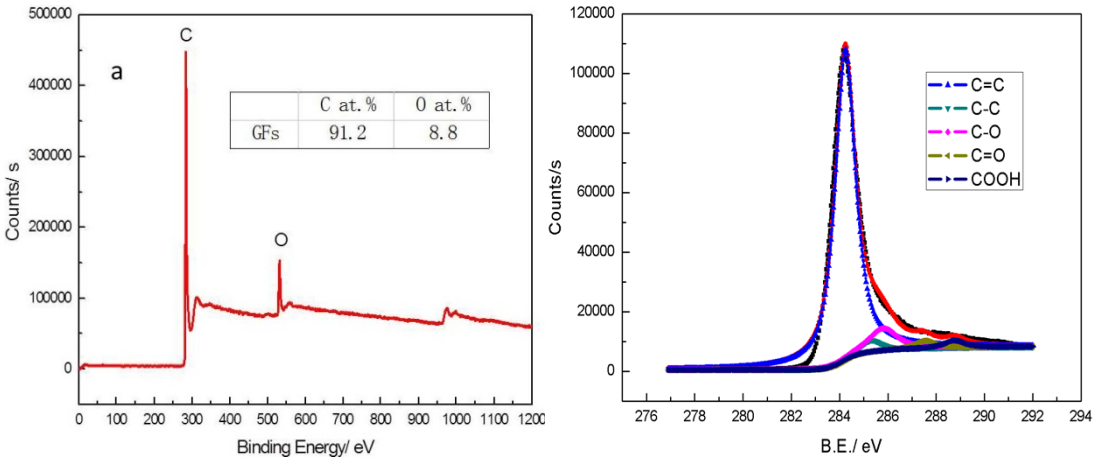

Figure S5. a, Survey scanned XPS spectrum of the GFs obtained from the fast decomposition of NaAc at 1200 °C, showing oxygen atoms are involved in the GFs. b, high-resolution C1s spectrum for the GFs. Five types of bonding conjugations, 284.2 eV (C=C), 285.3 eV (C-C), 285.8 eV (C-O), 287.6 eV(C=O) and 288.9 eV (O-C=O), can be well fitted by spectrum deconvolution .[10-12]

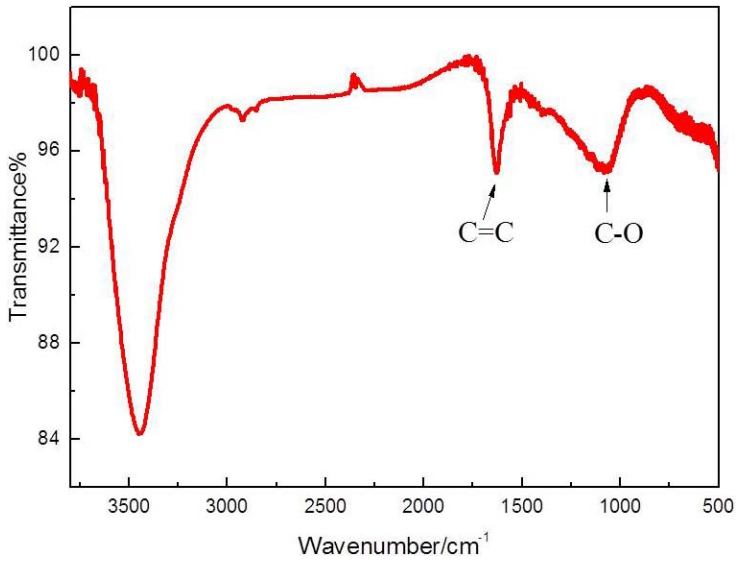

Figure S6. FTIR spectrum of the GFs obtained from the fast decomposition of NaAc at 1200 °C, showing a strong C=C stretching vibration at 1636 cm^{-1} and a C-O stretching vibration at 1070 cm^{-1}.[13]

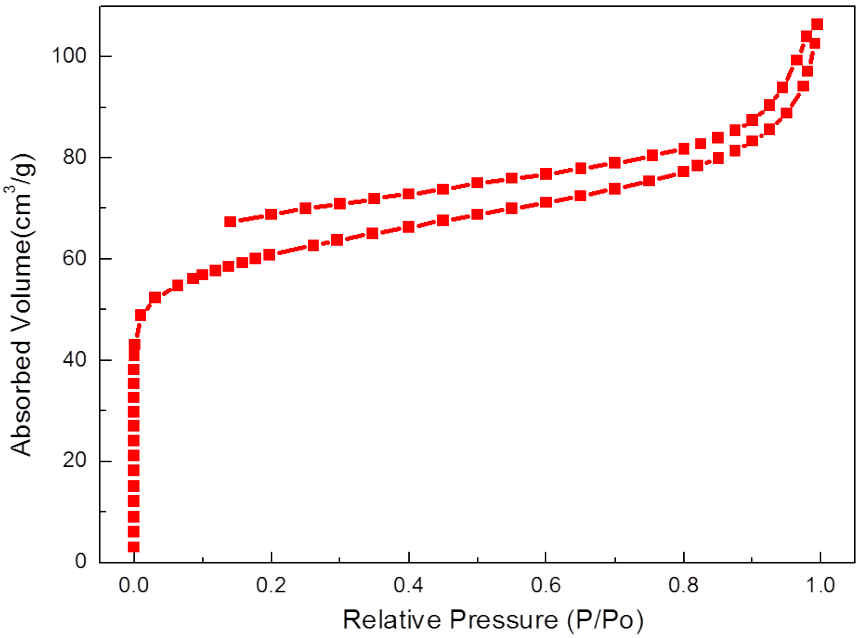

Figure S7. N_2 adsorption isotherms of the GFs obtained from the fast decomposition of NaAc at 1200 °C.

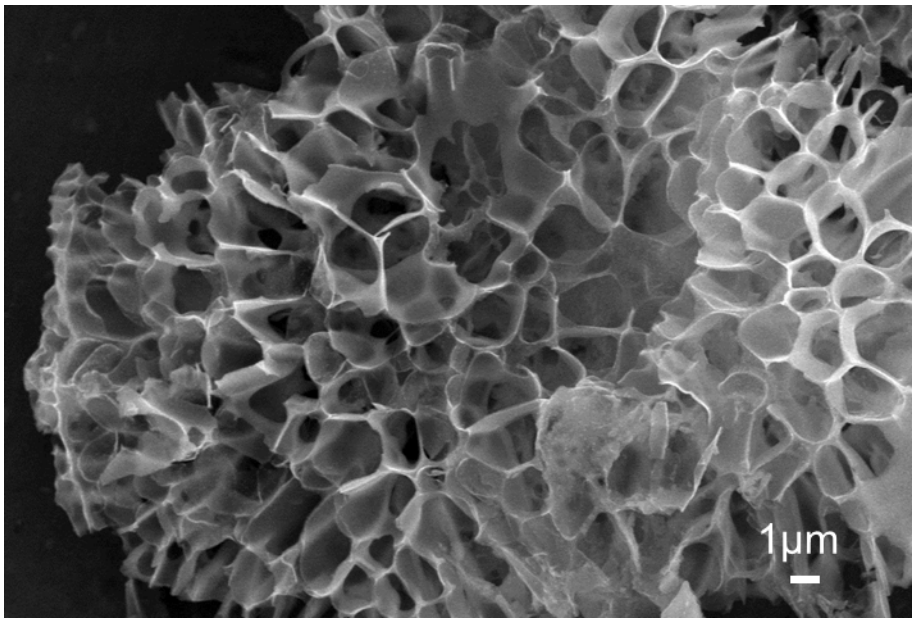

Figure S8. SEM image of the sample obtained by post-annealing of GFs at 1200 ^{o}C for 1h.

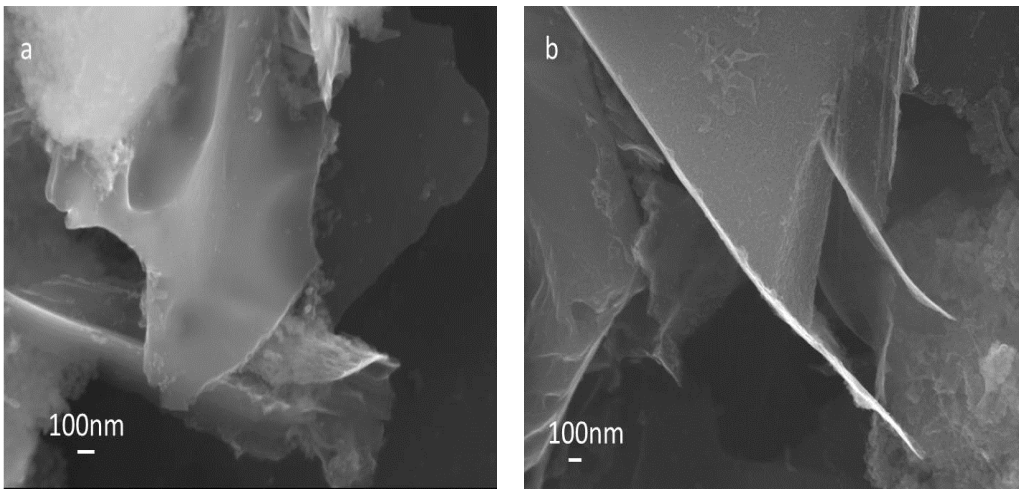

Figure S9. SEM images of the sample obtained from a temperature-programmed decomposition of NaAc. Heating rate, 10 ^{o}C/min; final temperature, 800^{o}C.

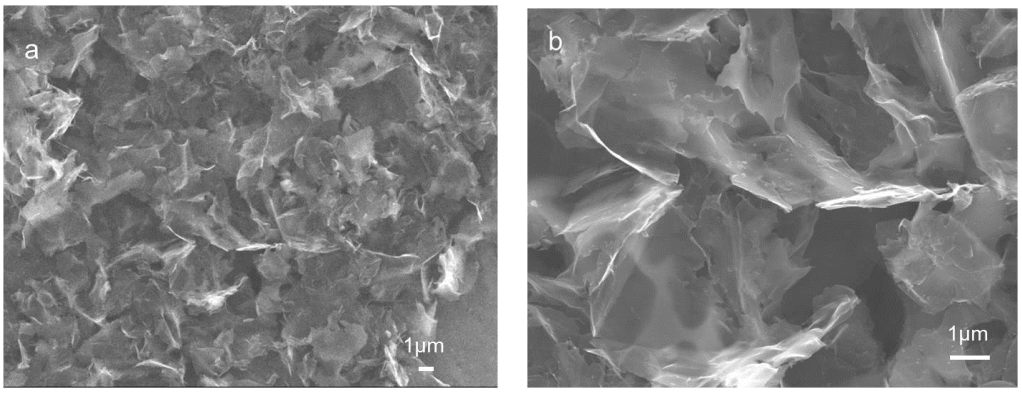

Figure S10. SEM images of the sample obtained from a fast decomposition of NaAc at 700 ^{o}C.

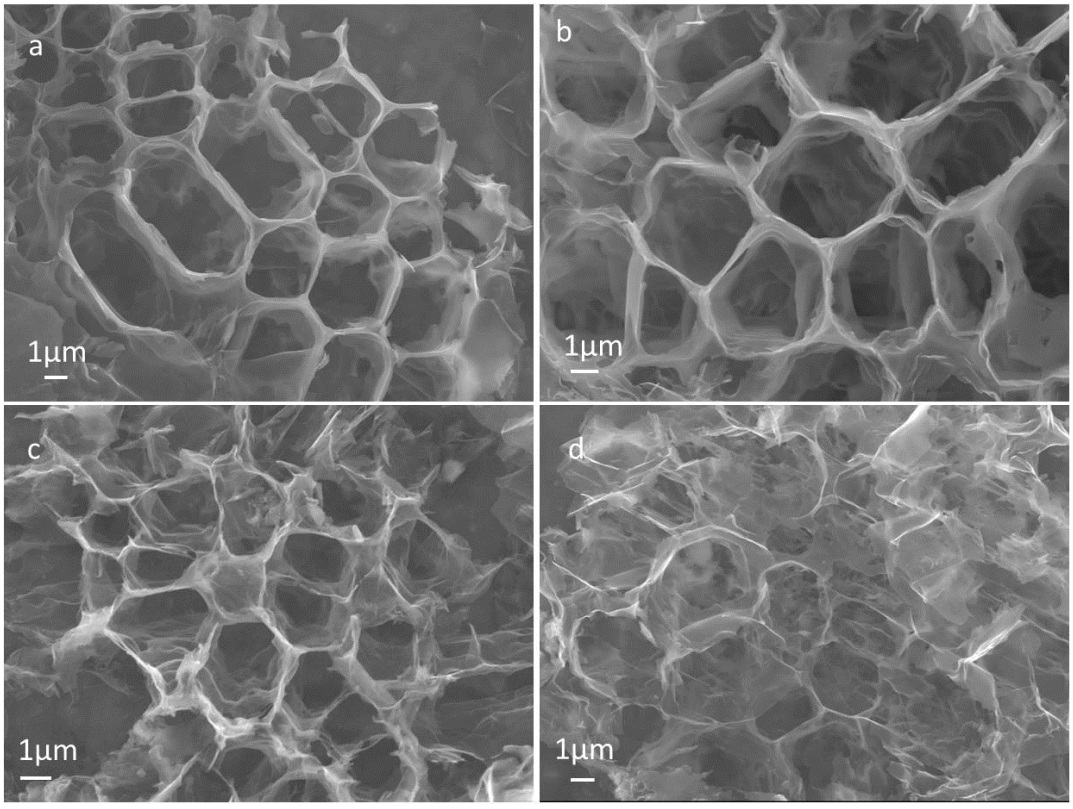

Figure S11. SEM images of the samples obtained from the fast decomposition of NaAc at 800 ^{o}C (a), 900 ^{o}C (b), 1000 ^{o}C (c), and 1100 ^{o}C (d).

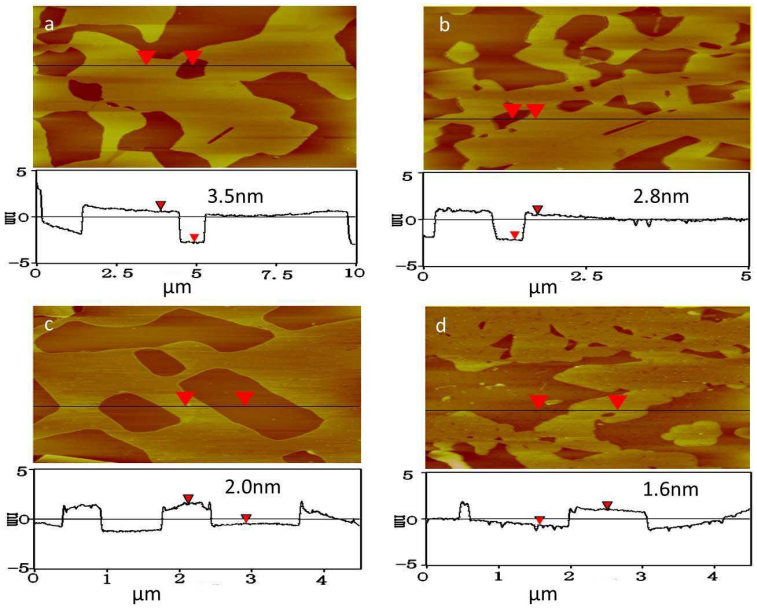

Figure S12. AFM images of the samples obtained from the fast decomposition of NaAc at 800 °C (a), 900 °C (b), 1000 °C (c), and 1100 °C (d).

During the fast pyrolysis of NaAC, the Na_2CO_3 core was formed. The Na_2CO_3 particles can possess the function of activation to produce pores, such as the role of KOH using in graphene activation.[14] Therefore, it is quite possible to appear pores in the graphene sheets. As shown in the SEM images of GFs (Figure S11), the graphene sheets which constructed the framework structures were not unbroken sheets but with large pores. So when tested by AFM, the obtained images were possible to have pores.

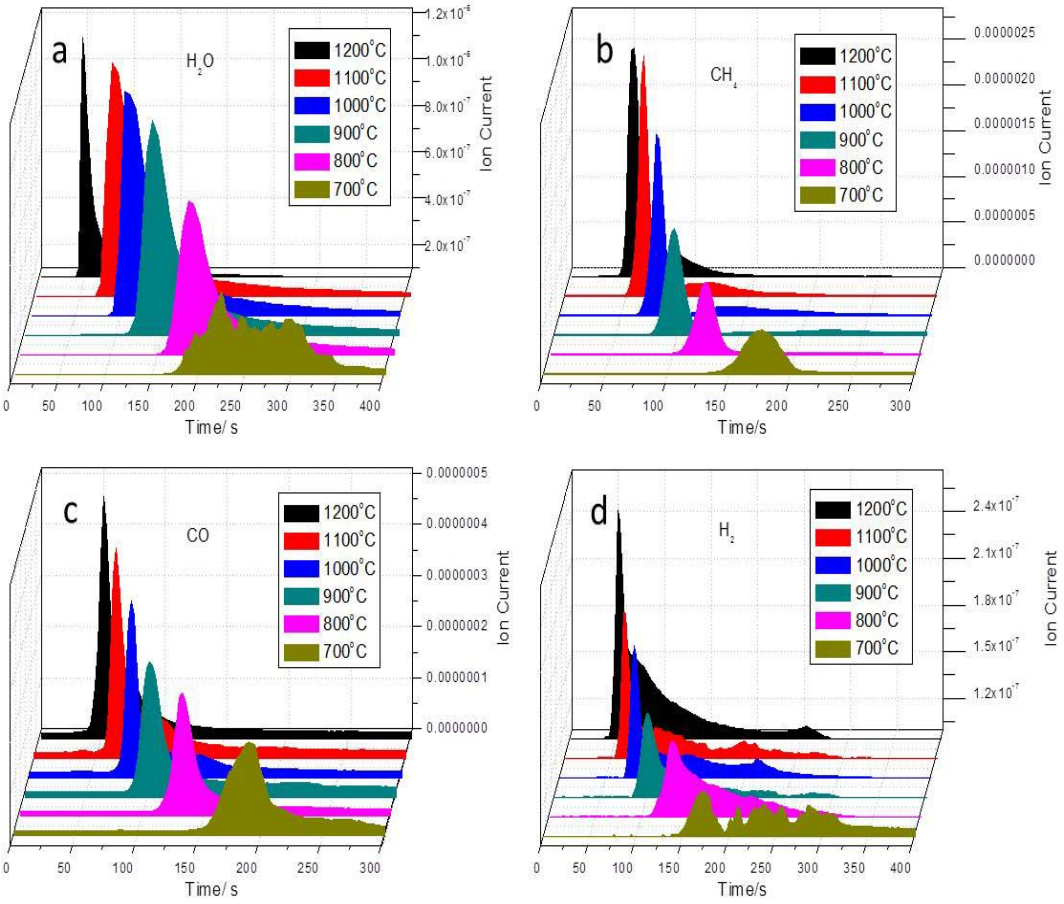

Figure S13. Mass spectrometry cycles obtained over the duration of heating emphasising different fragments during fast decomposition of NaAc at different temperatures. a, 18 amu fragments (H_2O); b, 16 amu fragments (CH_4); c, 28 amu fragments (CO); d**,** 2 amu fragments (H_2).

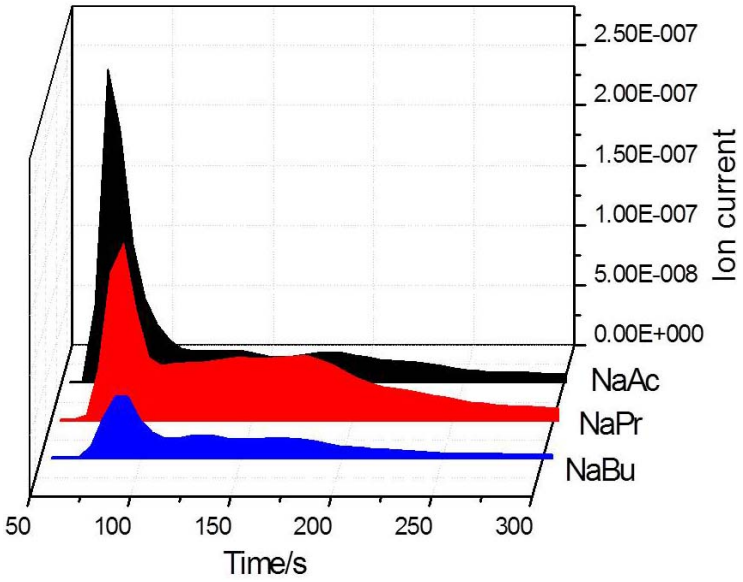

Figure S14. Mass spectrometry cycles obtained over the duration of heating emphasising 44 amu fragments (CO_2) during fast decomposition of NaAc, NaPr and NaBu at 1000 ^{o}C. It indicates that NaPr and NaBu release less gases under the same conditions.

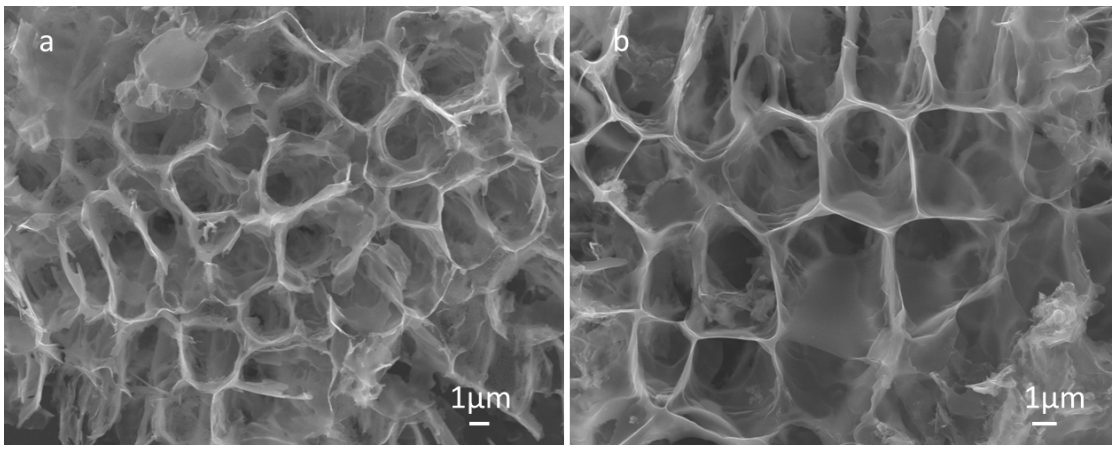

Figure S15. SEM images of the products obtained from the fast decomposition of NaPr **(a)** and NaBu **(b)** at 1200 ^{o}C.

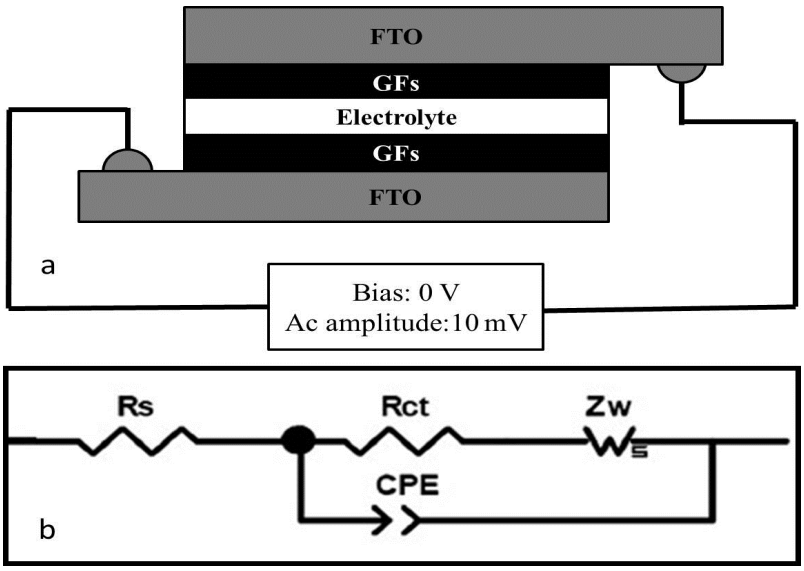

Figure S16. a, Schematic diagram of the symmetric cell for the analyses of counter electrodes with electrochemical impedance spectroscopy. **b,** Equivalent circuit diagram used to fit the observed impedance spectra.

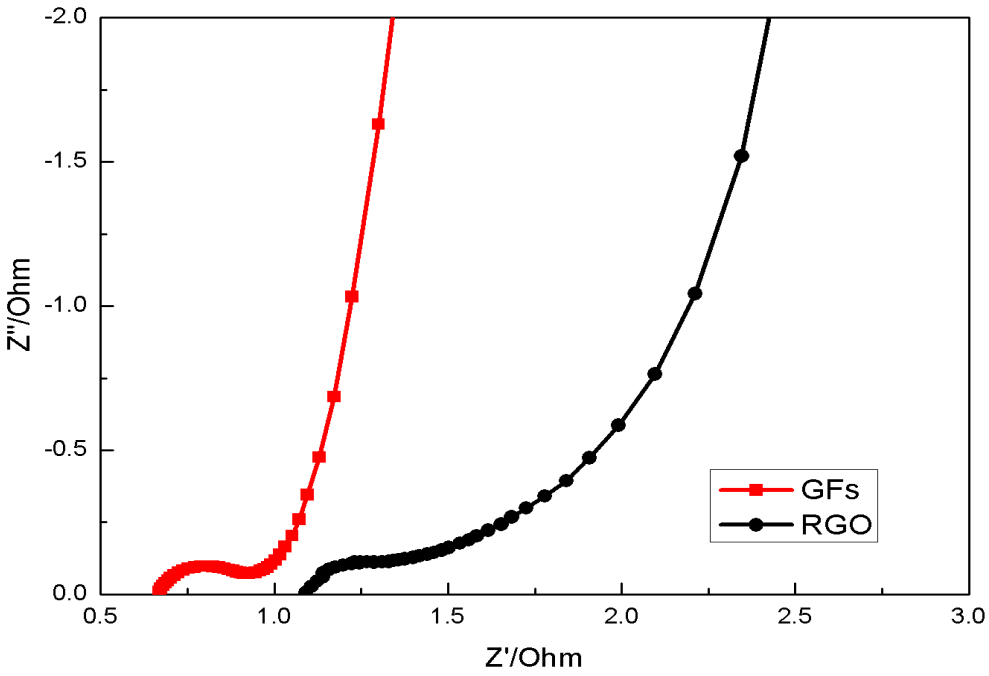

Figure S17. Nyquist plots of the GFs and RGO-modified electrodes in 6 M KOH.

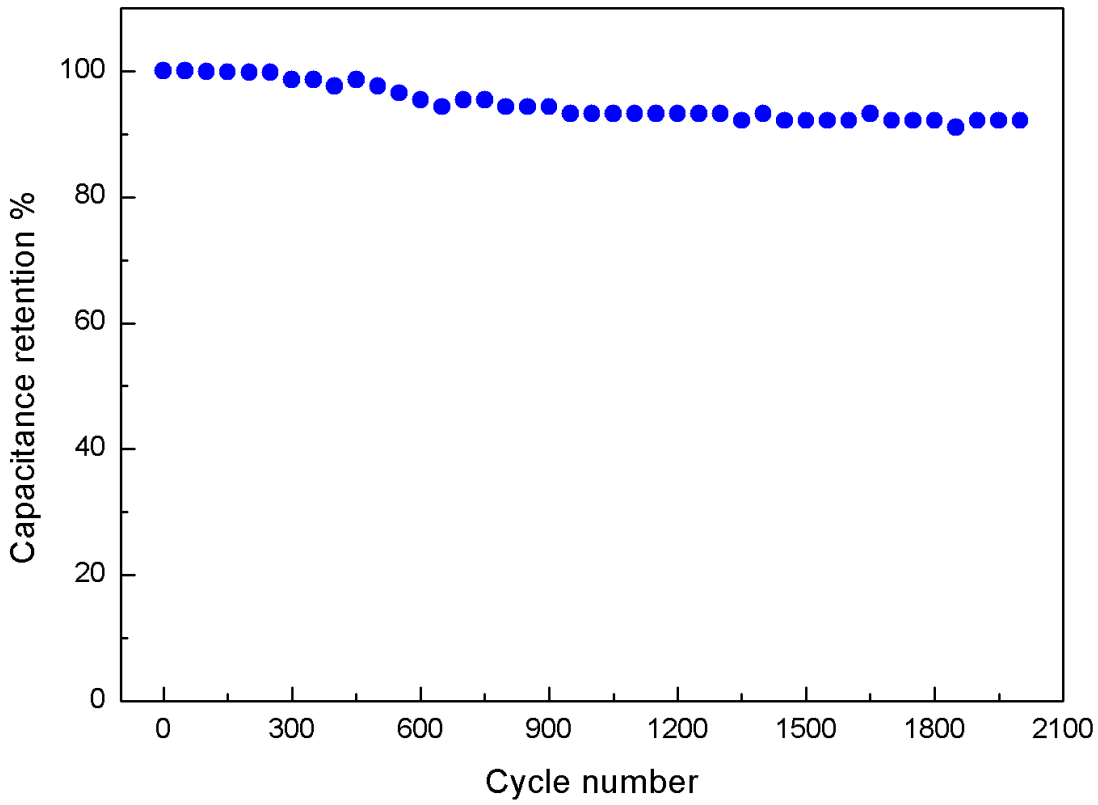

Figure S18. Cycle stability of the GFs-modified electrode at a current density of 2 A g^{-1} in supercapacitor.

Table S1. The comparisons of preparation methods of 3D graphene.

3D graphene	Methods	Reactants	Templates	Preparation processes	References
3D foam-like graphene	CVD	CH_4	nickel foams	One-step	*Nat. Mater.*, 2011,**10**, 424.
3D graphene aerogels	Freeze-drying	GO		Multi-step	*J.Am. Chem. Soc.,* 2012, **134**, 19532. *Angew. Chem. Int. Ed.,* 2012, **51**, 11371.
Macroporous graphene	Template-assisted	GO	PS/ PMMA	Multi-step	*Chem. Commun.,* 2012, **48**, 714 *ACS Nano.,* 2012, **6**, 4020.9.
Ordered Mesoporous Graphene Frameworks	Template-assisted	oleic acid	Fe_3O_4	Multi-step	*Angew. Chem. Int. Edit.,* 2015, **54,** 5727. *Nat. Commun.*, 2015, **6**, 6420.
GFs	Fast pyrolysis	Organic Sodium Salt	Na_2CO_3 (In-situ)	One-step	Our work

There were some excellent reports on the synthesis of 3D graphene.[15-22] However, our method was quite different from those methods and possessed obvious innovations. The detailed comparisons were given in Table S1.

3D foam-like graphene macrostructures were synthesized with nickel foams as template by chemical vapor deposition.[15] To use the 3D foam-like graphene in practical application, the nickel foam template needs to be etched away and could not be renewed, which is unfavorable for large scale synthesis. 3D graphene aerogels were prepared by hydrothermal assembly of graphene oxide in an aqueous suspension, followed by a freeze-drying process.[16,17] As graphene oxides were initially prepared by the modified Hummers method, which should use serious reagents such as concentrated sulfuric acid and potassium permanganate, the process was inherently hazardous. Besides, as the prepared progresses were multistep, it was time-consuming. Macroporous graphene were fabricated by using polymethyl methacrylate latex spheres (PMMA) or polystyrene spheres (PS) as sacrificial templates.[18,19] The synthesis cost was increased owing to the multistep processes and the use of sacrificial templates. Highly ordered mesoporous graphene frameworks were enabled by Fe_3O_4 nanocrystal superlattices.[20,21] This synthesis method was multistep, including synthesis of monodisperse Fe_3O_4 NCs, self-assembly Fe_3O_4 NC superlattices and fabrication of MGFs, which made the synthesis more time-consuming. Compared with these methods, the GFs synthetized by our method had several features as follows. First, the synthesis process was one-step and fast (typically one or two minutes), which made it more time-saving. Second, the Na_2CO_3

template was formed in-situ, which can be removed by simply water-washing (harsh etching agents such as strong acids or strong oxidants were avoided). Besides, the Na_2CO_3 particles after washing can be recovered easily by recrystallization. The recovered Na_2CO_3 particles could react with acetic acid to form NaAC, which can be used to synthetize GFs again. Third, the reactant (NaAC) is common reagent which is cheap and non-toxic. Therefore, compared with these methods, our method is simple, green, cheap and time-saving, which is quite possible to large scale synthesis and applications.

Compared with 3D graphene synthesized through other methods,[16,18,22-24] the electrode performance of GFs synthesized by our method was also kept at high levels. As the little lower performance of GFs (compared with some previous reports[17,25]), it may be resulted from the different structures of 3D graphene such as pore structure, oxygen-containing groups and so on. The speculation will be studied in the future work. Anyhow, overall consideration of the simple, green, cheap and time-saving synthesis method, the GFs is a promising and competitive electrode material.

Table S2. Electrochemical parameters for different counter electrodes and the photovoltaic parameters of the corresponding QDSSCs

CE	V_{oc} (V)	J_{sc} (mA/cm^2)	FF (%)	η (%)	R_s (Ω·cm^2)	R_{ct} (Ω·cm^2)	Z_N (Ω·cm^2)
GFs	0.56	13.86	45.80	3.57	3.77	2.07	3.63
RGO	0.51	12.57	40.71	2.58	4.80	17.84	15.52
Pt	0.58	12.65	41.48	3.03	3.77	163.36	12.34

The diffusion component in the platinum electrode was not evident in Figure 4a, attesting to the sluggish kinetics with this electrode which leaded to quite large charge-transfer impedance (163.36 Ω·cm^2). This result was similar with the previous reports.[26,27] That is also one of the reasons to find other materials to replace platinum in QDSSCs. The GFs exhibited slight charge-transfer impedance and diffusion impedance, further supporting the good charge-transfer and diffusion abilities.

Table S3. Electrochemical impedance parameters for GFs and RGO-modified electrodes in 6 M KOH.

Electrode	R_s (Ω)	R_{ct} (Ω)	Z_N (Ω)
GFs	0.61	0.37	0.56
RGO	1.14	0.53	2.63

By fitting the Nyquist plots with an equivalent circuit model, the series resistance (R_s), charge transfer resistance (R_{ct}) at the electrode–electrolyte interface, and Nernst diffusion impedance (Z_N) were extracted. Obviously, the R_s, R_{ct}, and Z_N values of the GFs electrode were much lower than those of the RGO electrode. This result revealed the multiple promotion effects involved in the GFs. The small R_s of GFs-modified electrode was attributed to the framework structure which can provide multi-direction channels for electron conduction. The small Z_N of the GFs-modified electrode indicated the fast diffusion rate of electrolyte ions.

References

1 T.H. Tsai, S.C. Chiou, S.M. Chen, *Int. J. Electrochem. Sci,* 2011, **6**, 3333.

2 J. Luo, H. Wei, Q. Huang, X. Hu, H. Zhao, R. Yu, D. Li, Y. Luo, Q. Meng, *Chem. Commun.,* 2013, **49**, 3881.

3 N. Papageorgiou, W. Maier, M. Grätzel, *J. Electrochem. Soc.,* 1997, **144**, 876.

4 J. Chen, B. Li, J. Zheng, J. Zhao, Z. Zhu, *J. Phys. Chem. C,* 2012, **116**, 14848.

5 J. Dong, S. Jia, J. Chen, B. Li, J. Zheng, J. Zhao, Z. Wang, Z. Zhu, *J. Mater. Chem.*, 2012, **22**, 9745.

6 A. C. Ferrari, D. M. Basko, *Nat. Nanotechnol.,* 2013, **8**, 235.

7 D. Kim, J. Y. Han, D. Lee, Y. Lee, D. Y. Jeon, *J. Mater. Chem.,* 2012, **22**, 20026.

8 C. Nethravathi, M. Rajamathi, *Carbon*., 2008, **46**, 1994.

9 C. Chen, W. Fan, T. Ma, X. Fu, *Ionics.*, 2014, **20**, 1489.

10 K. László, E. Tombácz, K. Josepovits, *Carbon,* 2001, **39**, 1217.

11 H. Wang, K. Sun, F. Tao, D. J. Stacchiola, Y. H. Hu, *Angew. Chem. Int. Ed.*, 2013, **52**, 9210.

12 W. Zhang, J. Cui, C.a. Tao, Y. Wu, Z. Li, L. Ma, Y. Wen, G. Li, *Angew. Chem. Int. Ed.,* 2009, **48**, 5864.

13 D. Zhou, Q.Y. Cheng, B.H. Han, *Carbon,* 2011, **49**, 3920.

14 Y. Zhu, S. Murali, M. D. Stoller, K. J. Ganesh, W. Cai, P. J. Ferreira, A. Pirkle, R. M. Wallace, K. A. Cychosz, M. Thommes, D. Su, E. A. Stach, R. S. Ruoff, *Science*, 2011, **332**, 1537.

15 Z.P. Chen, W.C. Ren, L.B. Gao, B.L. Liu, S.F. Pei, H.M. Cheng, *Nat. Mater.*, 2011,**10**, 424.

16 Z. S. Wu, Y. Sun, Y. Z. Tan, S. Yang, X. Feng, K. Mullen, *J.Am. Chem. Soc.,* 2012, **134**, 19532.

17 Y. Zhao, C. Hu, Y. Hu, H. Cheng, G. Shi, L. Qu, *Angew. Chem. Int. Ed.,* 2012, **51**, 11371.

18 C. M. Chen, Q. Zhang, C. H. Huang, X. C. Zhao, B. S. Zhang, Q. Q. Kong, M. Z. Wang, Y. G. Yang, R. Cai, D. Sheng Su, *Chem. Commun.*, 2012, **48**, 7149.

19 B. G. Choi, M. Yang, W. H. Hong, J. W. Choi, Y. S. Huh, *ACS Nano.*, 2012, **6**, 4020.

20 Y. Jiao, D. Han, L. Liu, L. Ji, G. Guo, J. Hu, D. Yang, A. Dong, *Angew. Chem. Int. Ed.,* 2015, **54**, 5727.

21 Y. Jiao, D. Han, Y. Ding, X. Zhang, G. Guo, J. Hu, D. Yang, A. Dong, *Nat. Commun.,* 2015, **6**, 6420.

22 Chen, C. M.; Zhang, Q.; Zhao, X. C.; Zhang, B.; Kong, Q.Q.; Yang, M.-G.; Yang, Q.H.; Wang, M.Z.; Yang, Y.G.; Schlögl, R.; Su, D. S. *J. Mater. Chem.* 2012, **22**,14076.

23 H. S. Ahn, J. W. Jang, M. Seol, J. M. Kim, D. J. Yun, C. Park, H. Kim, D. H. Youn, J. Y. Kim, G. Park, S. C. Park, J. M. Kim, D. I. Yu, K. Yong, M. H. Kim, J. S. Lee, *Sci. Rep.,* 2013, **3**,

1396.

24 P. Parand, M. Samadpour, A. Esfandiar, A. I. Zad, *ACS Photonics,* 2014, **1**, 323.

25 J. Hu, Z. Kang, F. Li, X. Huang, *Carbon*, 2014, **67**, 221.

26 M. Ye, C. Chen, N. Zhang, X. Wen, W. Guo, C. Lin, *Adv. Energy Mater.*, 2014, **4**. 1301564

27 J. G. Radich, R. Dwyer, P. V. Kamat, *J. Phys. Chem. Lett.,* 2011, **2**, 2453.